catalysts

MDPI

Article

Roles of Nanostructured Bimetallic Supported on Alumina-Zeolite (AZ) in Light Cycle Oil (LCO) Upgrading

Jianglong Pu [1,†], Haiping Zhang [2,3,†], Min Wang [4], Kyle Rogers [2], Hongmei Wang [1], Hui Wang [1,2,*], Siauw Ng [5] and Ping Sun [1,*]

1 College of Biological, Chemical Sciences and Engineering, Jiaxing University, 118 Jiahang Road, Jiaxing 314001, China; longpu@zjxu.edu.cn (J.P.); wanghongmei@zjxu.edu.cn (H.W.)
2 Department of Chemical Engineering, University of New Brunswick, 15 Dineen Drive, Fredericton, NB E3B 5A3, Canada; hpzhang@tju.edu.cn (H.Z.); kyle_allen.rogers@unb.ca (K.R.)
3 Department of Chemical Engineering & Technology, Tianjin University, Tianjin 300072, China
4 School of Petroleum Engineering & Environment, Zhejiang Ocean University, 1 South Haida Road, Lincheng Changzhi Island, Zhoushan 316022, China; wangmin@zjou.edu.cn
5 National Centre for Upgrading Technology, Canmet ENERGY-Devon, 1 Oil Patch Drive, Edmonton, AB T9G 1A8, Canada; siauw.ng@canada.ca
* Correspondence: huiwang@zjxu.edu.cn (H.W.); sunping@zjxu.edu.cn (P.S.)
† As the co-first author.

Abstract: Light cycle oil (LCO) is one of the major products in Fluid catalytic cracking (FCC) processes, and has drawbacks such as high aromatics, sulfur, and nitrogen contents, and low cetane number (CN). Hydro-upgrading is one of the most typical processes for LCO upgrading, and alumina-zeolite (AZ) is an effective hydrotreating catalyst support. This paper examined the effects of different bimetallic catalysts (CoMo/AZ, NiMo/AZ, and NiW/AZ) supported by AZ on hydro-upgrading of both model compounds and real LCO. CoMo/AZ preferred the direct desulfurization (DDS) route while the NiMo/AZ and NiW/AZ catalysts favored the desulfurization route through hydrogenation (HYD). The presence of nitrogen compounds in the feed introduced a competitive adsorption mechanism and reduced the number of available acid sites. Aromatics were partially hydrogenated into methyltetralines at first, and then further hydrogenated, cracked, and isomerized into methyldecalins, monocyclic, and methyltetralines isomers. CoMo/AZ is the best hydrodesulfurization (HDS) catalyst for the model compounds at low H_2 pressure (550 psi) and for LCO at lower temperature (573 K), while NiMo/AZ performs the best for LCO at higher temperature (648 K). NiMo/AZ is the best hydrodenitrogenation (HDN) catalyst for LCO. The hydrodearomatization (HDA) performances of NiMo/AZ and NiW/AZ improved significantly and overwhelmingly higher than that of the CoMo/AZ when the H_2 pressure was increased to 1100 psi.

Keywords: bimetallic; alumina-zeolite support; light cycle oil; hydrodesulfurization; hydrodenitrogenation; hydrodearomatization

Citation: Pu, J.; Zhang, H.; Wang, M.; Rogers, K.; Wang, H.; Wang, H.; Ng, S.; Sun, P. Roles of Nanostructured Bimetallic Supported on Alumina-Zeolite (AZ) in Light Cycle Oil (LCO) Upgrading. *Catalysts* **2021**, *11*, 1277. https://doi.org/10.3390/catal11111277

Academic Editors: Eduard Karakhanov and Aleksandr Glotov

Received: 22 August 2021
Accepted: 19 October 2021
Published: 22 October 2021

1. Introduction

Heavy oil has to be upgraded before utilization because of high density and high boiling point. Fluid catalytic cracking (FCC) is one of the most important means to transforming heavy oil into high value-added products, such as gasoline distillates. Light cycle oil (LCO) is another major product in FCC processes, accounting for 10–30% FCC products and more than one third of the distillate pool in China, whose density and boiling point are close to that of diesel fractions [1–4]. With aromatics contents between 75% and 85% (especially polycyclic aromatic hydrocarbons (PAH), which account for 40% to 50%), sulfur and nitrogen contents up to 1.5 wt% and 0.3 wt%, and cetane number (CN) less than 35; LCO cannot be directly used as diesel fractions [3,4]. Instead, LCO is used as a blending component for diesel fuel, heating, or fuel oils [2]. Because of the crude oil deteriorates, the quality of LCO become even worse. Nowadays, with the public's increasing awareness

of the environmental protection, the standards of fuel oil are becoming more and more stringent. By now, the sulfur content is expected to be lowered to 10 ppm in most developed countries and some developing countries. The standard for automobile diesel fuels in China has also been restricted to a maximum Polycyclic aromatic hydrocarbons (PAH) content of 7 wt% and a minimum CN of 47.

Hydrotreating is one of the most typical processes for LCO upgrading [2]. Aromatics saturation, ring opening, and sulfur/nitrogen-containing compound removal are the primary reactions during the hydrotreating process. However, it is hard to remove the refractory aromatics and sulfur/nitrogen-containing compounds from LCO using the conventional hydrotreating catalysts and processes. For example, the active amount of the traditional HDS catalyst has to increase fourfold to remove 90% of the sulfur in diesel fractions at 500 ppm [5]. Consequently, developing new technologies for LCO upgrading is desirable [2,3]. It is time-consuming and expensive work comparing or improving effective catalysts; the latter may be a better choice. The essential approaches for developing catalysts including developing novel supports, exploiting new active metal components, and tailoring the catalyst acidity [6–8]. Our previous studies revealed that [9–17]: (1) Mo (W) sulfides promoted by Ni (Co) promoter are good active metals for the LCO hydrotreating process; (2) The addition of zeolite components such as zeolite beta, zeolite Y, and ZSM-5 in the support matrix of the hydrotreating catalysts led to the enhancement in its HDN, HDS, and HDA performances; and (3) the addition of the combination of zeolite beta and Y in the support matrix of hydrotreating catalysts had achieved better performances than single zeolite beta or Y. In this work, alumina-zeolite (AZ) supported CoMo, NiMo, and NiW catalysts were synthesized and evaluated using model compounds, and real LCO as feedstocks. The compositions of hydrotreated liquids were determined by Gas chromatography/Flame Ionization Detector- Pulsed flame photometric detector (GC/FID-PFPD), Gas chromatography and mass spectrometry (GC/MS), and High performance liquid chromatography (HPLC). Catalyst acidity, morphology, and textural properties were analyzed using X-ray diffraction (XRD), pyridine-Fourier transform infrared spectroscopy (FTIR), X-Ray Photoelectron Spectroscopy (XPS), and Transmission electron microscopy (TEM), whose purpose is to upgrade LCO by means of HDS, HDN, and HDA into a premium diesel blending component over a AZ supported bimetallic catalysts. The study aims to examine the effects of NiMo, NiW, and CoMo supported by AZ on the catalytic performance in the hydro-upgrading process.

2. Results and Discussion

2.1. Catalyst Characterization

2.1.1. Texture Structures

Figure 1 shows the isotherm linear plots and pore-size distributions of the NiMo/AZ, CoMo/AZ, and NiW/AZ catalysts.

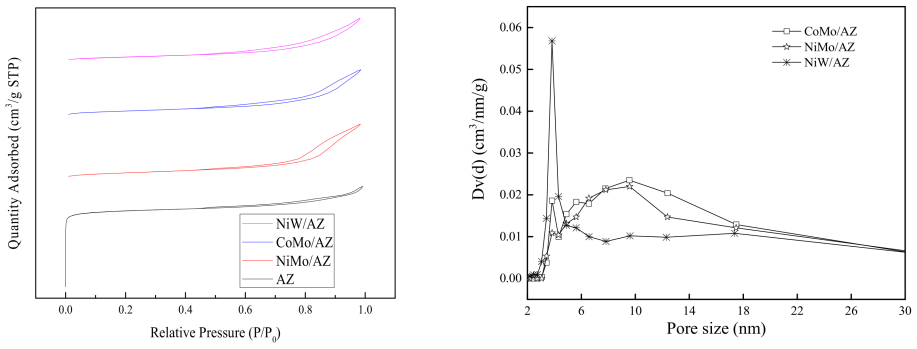

(**a**) (**b**)

Figure 1. Physical properties of the catalysts. (**a**) Isotherm linear plot; (**b**) Pore size distribution.

It can be seen from Figure 1a that the surface structures of AZ changed significantly after the active metals loaded. The isotherm of AZ is type I, rich of the microporous structure. An obvious hysteresis loop appeared on the isotherms curves after the active components were loaded on AZ; therefore, the adsorption and desorption curves of the supported catalysts are of type IV, mainly mesoporous structures.

As shown in Figure 1b, all three catalysts showed two kinds of pore structures, consisting of a narrow pore distribution at the diameter of 3–4 nm and a wide range from 8 to 30 nm, respectively. The former is the inherent intra-aggregated pores that located inside the support particle, whereas the latter is the secondary inter-aggregated pores between the support particles. NiW/AZ has more fine intra-aggregated pores and less secondary pores than both NiMo/AZ and CoMo/AZ, suggesting that W atoms are more apt to occupy the larger pores, and too large to enter the fine pores.

Table 1 lists the physical properties of the NiMo/AZ, CoMo/AZ, and NiW/AZ catalysts.

Table 1. Textural properties of the catalysts.

Catalysts	NiMo/AZ	CoMo/AZ	NiW/AZ
S_{BET}, m^2/g	141	185	149
Total pore volume, cm^3/g	0.44	0.49	0.39
Micropore volume, cm^3/g	0.061	0.084	0.066
Average layer length, nm	5.10	6.11	8.40
Average layer number	1.74	1.79	1.52

Compared to CoMo/AZ and NiMo/AZ, NiW/AZ has smaller surface area and pore volume, because the relatively smaller atom, Ni, is easier to enter the pores of the support, and cover more surface area and occupy more micropores. The total pore volume of the NiW/AZ is obviously smaller than that of the NiMo/AZ catalyst, which is attributed to the blockage of large-size W atoms. The micropore volume of NiMo/AZ is similar to that of the NiW/AZ catalyst, suggesting that some Mo atom might also distribute on the intra-pores whereas the W atoms have difficulty doing so.

The XRD results are presented in Figure 2.

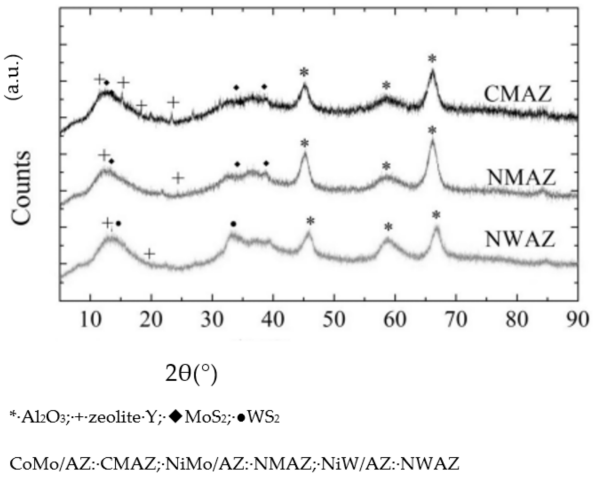

Figure 2. XRD profiles of the sulfided catalysts.

All three catalysts showed the existence of γ-Al_2O_3 and zeolite Y [9]. Ni and Co are uniformly distributed on the support as only trace MoS_2 and WS_2 peaks are observed in Figure 2.

2.1.2. Morphology

After being sulfided, Mo or W might form layered hexagonal MoS_2 or WS_2 structures, while Ni or Co atoms are located at the edges of MoS_2 and WS_2 slabs [18,19], which is shown in Figure 3.

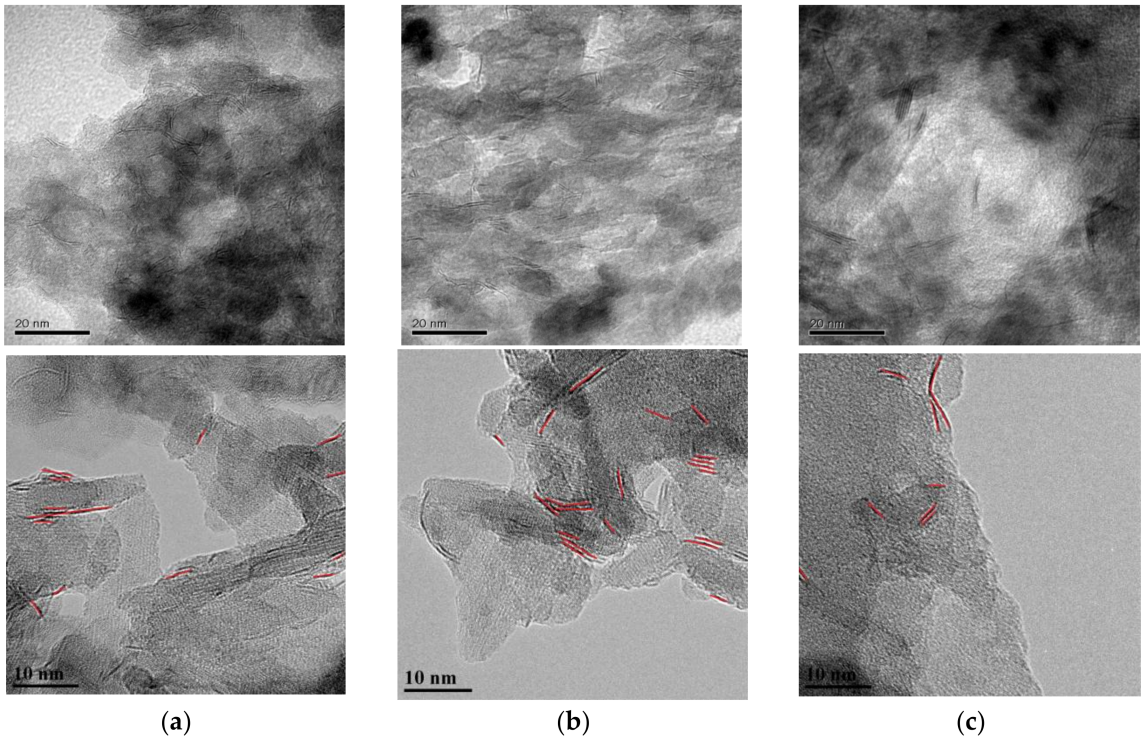

Figure 3. The representative TEM images of the sulfided catalysts. (**a**) CoMo/AZ; (**b**) NiMo/AZ; (**c**) NiW/AZ.

The average slab length was calculated using the same methods described in the previous publications [20]. The results are listed in Table 1. The length and layer number of the active clusters on sulfided catalysts are shown in Figure 4.

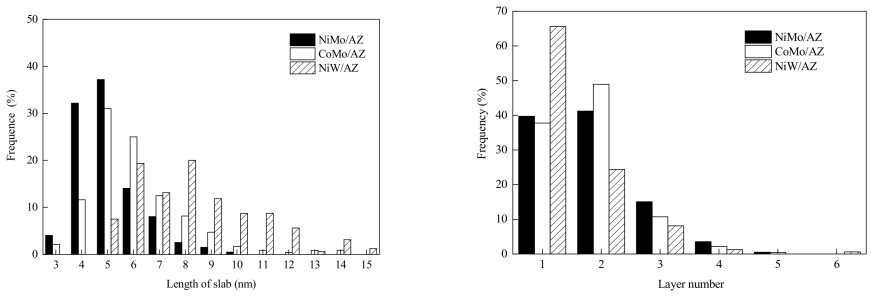

Figure 4. The properties of the slabs over the sulfided catalysts. (**a**) Length of Mo/WS_2 slabs; (**b**) Number of layers of the slabs.

As can be seen in Figure 4a, the average length of MoS_2 or WS_2 slabs decreases in the following order: NiW/AZ (8.40 nm) > CoMo/AZ (6.11 nm) > NiMo/AZ (5.10 nm). About two-thirds of the NiW/AZ slabs were evenly distributed between 6–9 nm. For the CoMo/AZ and NiMo/AZ catalysts, about 80% and more than 90% of the slabs were distributed between 4–7 nm respectively. For the slab layer shown in Figure 4b, NiMoS and CoMoS slabs are thicker than that of NiWS, most of which are single-layer slabs. This is because the precursor of W is in $W_{12}O_{40}{}^{6-}$ and Mo is in MoO_3. The former one may have a strong interaction with the protons on the zeolite support, resulting in a wider distribution

along the surface of the support. This enlarges the length of NiWS slab and reduces the number of slab layers. Comparing NiMo/AZ and CoMo/AZ; Ni atoms, which enter the zeolite channels more readily as they a smaller atomic radius, tend to be more evenly distribution across the support, and form more narrowly distributed NiMo/AZ slabs.

Figure 5 shows the states of S 2p and Mo 3d or W 4f on the sulfided catalysts.

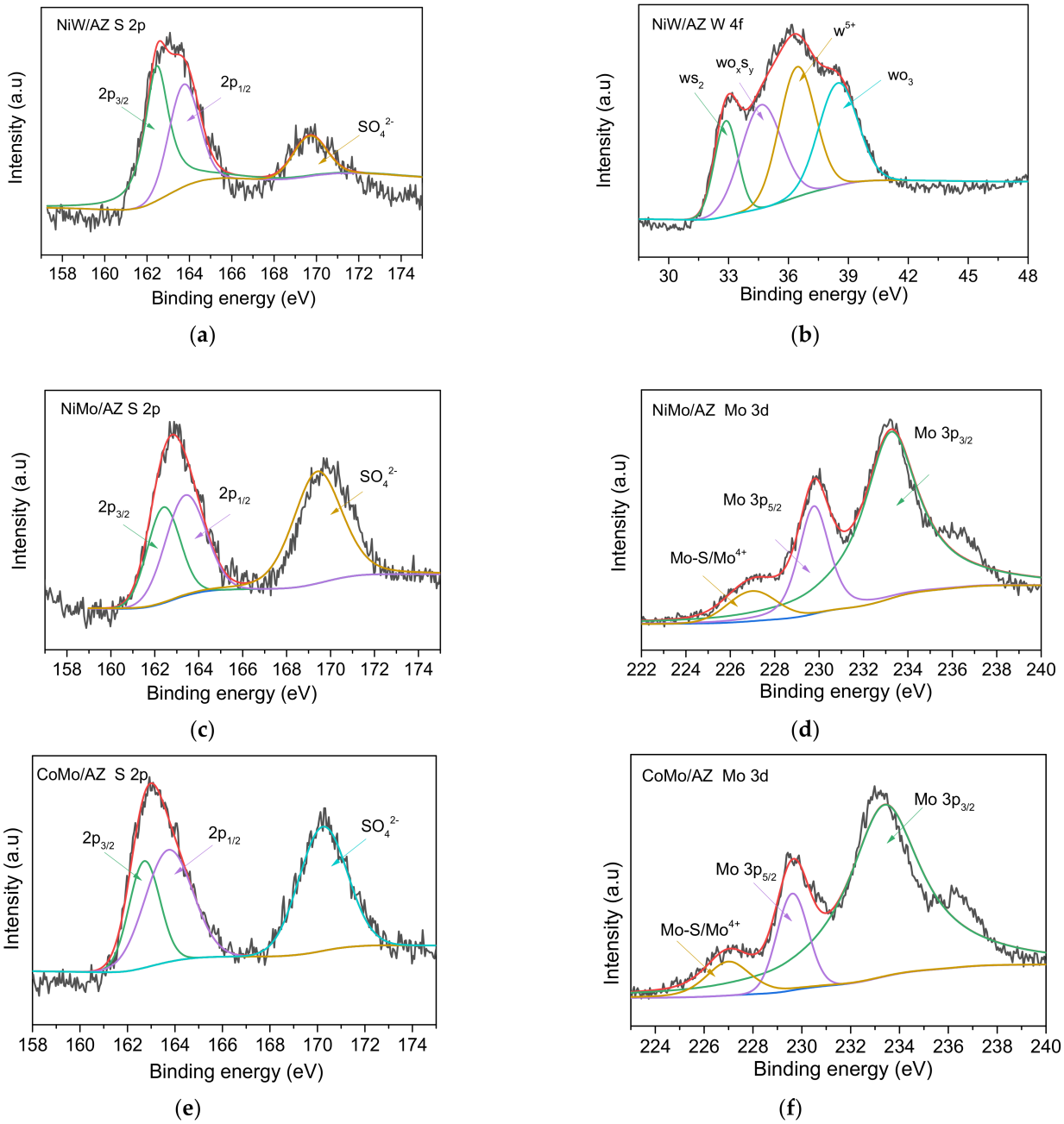

Figure 5. XPS spectra of the sulfided catalysts. (**a**) NiW/AZ S 2p; (**b**) NiW/AZ W 4f; (**c**) NiMo/AZ S 2p; (**d**) NiMo/AZ Mo 3d; (**e**) CoMo/AZ S 2p; (**f**) CoMo/AZ Mo 3d.

According to the literature [21–25], combining with the information in Figure 5, all these three catalysts exhibit the signals of both sulfur S $2p_{3/2}$ and MoS_2 or WS_2, and confirms the formation of sulfide phases on the catalysts, which is in accordance with the XRD results.

2.1.3. Acidity

Figure 6 shows the Pyridine-IR results of the NiMo/AZ and NiW/AZ catalyst before and after being sulfurized. Table 2 lists the B and L acid properties of the sulfided NiMo/AZ, CoMo/AZ, and NiW/AZ.

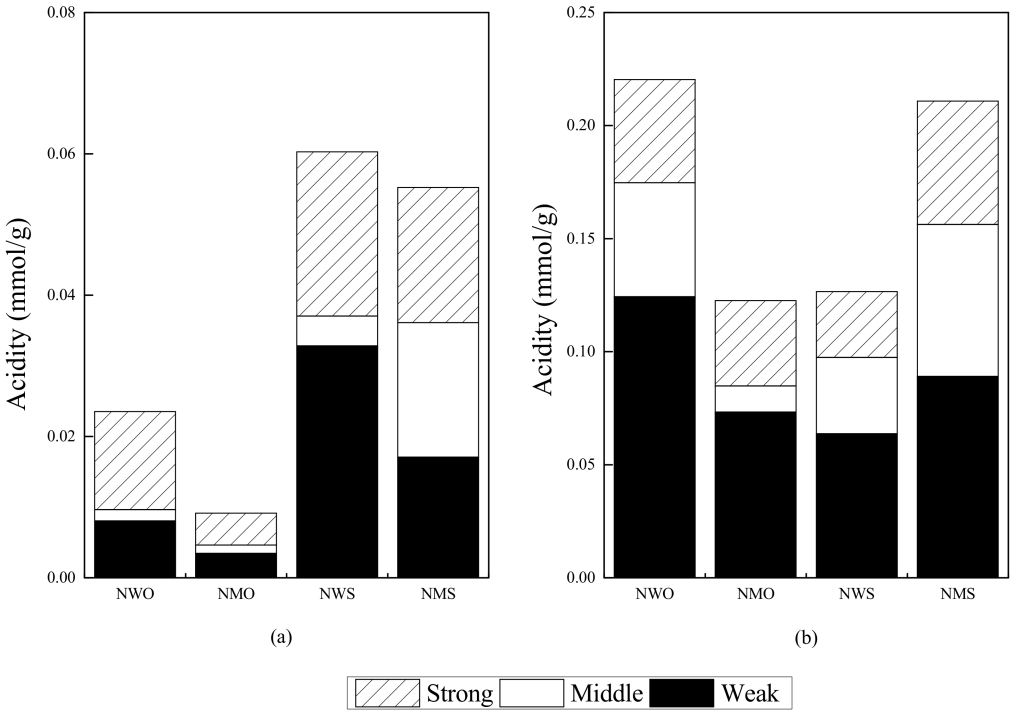

Unsulfided NiW/AZ: NWO; Unsulfided NiMo/AZ: NMO; Sulfided NiW/AZ: NWS; Sulfided NiMo/AZ: NMS

Figure 6. Acidic sites of the NiMo/AZ and NiW/AZ before and after sulfurization. (**a**) Bronsted acid; (**b**) Lewis acid.

Table 2. Acidic sites of the NiMoS/AZ, NiWS/AZ, and CoMoS/AZ catalysts.

Catalysts	B Acids, $\times 10^{-3}$ mmol/g				L Acids, mmol/g				Ratio of B/L			
	Weak	**Middle**	**Strong**	**Total**	**Weak**	**Middle**	**Strong**	**Total**	**Weak**	**Middle**	**Strong**	**Total**
NWS	32.8	4.2	23.3	60.3	63.7	33.7	29.1	126.5	0.52	0.13	0.80	0.48
NMS	17.1	19.0	19.1	55.2	89.1	67.2	54.5	210.8	0.19	0.28	0.35	0.26
CMS	18.0	16.0	13.8	47.8	21.0	15.2	9.2	45.4	0.86	1.05	1.50	1.05

The acidities of catalysts were calculated by the Pyridine FTIR results. For both the oxidized and sulfurized NiMo/AZ and NiW/AZ, the amount of Lewis acids is more than that of Brønsted acids. The amount of Brønsted acids increased greatly after being sulfurized. However, for the NiW/AZ catalyst, its Lewis acidity decreased after being sulfurized. Therefore, the sulfurized NiMo/AZ catalyst has a higher total acidity than the NiW/AZ.

As can be seen in Table 2, The total B acids on the three catalysts barely have a difference, but it is not the case for L acids, which on NiMo/AZ is nearly twofold and fourfold greater to that of the NiW/AZ and CoMo/AZ. As to acid types, the acids on both NiMo/AZ and NiW/AZ are mainly L acids, especially for the former; whereas the B and L acids on CoMo/AZ are basically the same. In the terms of acid strength, the acids on NiW/AZ are mainly weak acids, and those on CoMo/AZ are mostly weak and middle acids, while there is an equal distribution of weak, middle, and strong acids on NiMo/AZ.

2.2. Reaction Performances

The hydrotreating reaction performances of NiMo/AZ, CoMo/AZ, and NiW/AZ were carried out on both model oil and real LCO feeds. The model oil consists of 4,6-DMDBT, carbazole, and 1-methyl naphthalene. For LCO feed, the contents of the total S, the total N, and the total aromatics remaining in the hydrotreated products were respectively correlated with HDS, HDN, and HDA performances.

2.2.1. Model Compounds as Feed

HDS Performance

Figure 7 describes how the amounts of the 4,6-dimethyldibenzothiophenes (4,6-DMDBT), 4-methyldibenzothiophenes (4-MDBT), and 3,6-dimethyldibenzothiophenes (3,6-DMDBT) varied with time-on-stream over the CoMo/AZ catalyst.

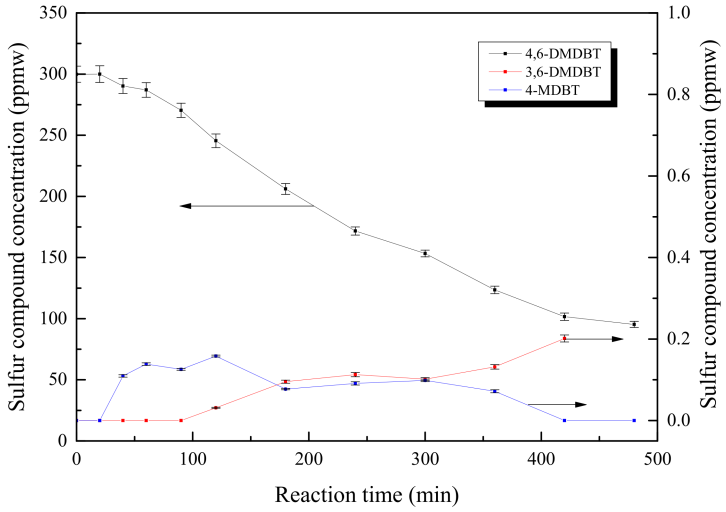

Figure 7. The conversion of 4,6-DMDBT and the formation of 4-MDBT and 3,6-DMDBT with time on stream over CoMo/AZ (Reaction conditions: 648 K, 8.96 MPa, 1000 rpm, 20 g catalyst, 200 g feed (4,6-DMDBT with 300 ppm sulfur in Hexadecane).

4,6-DMDBT decreased slightly in the initial 60 min and then decreased linearly from 290 ppm at 60 min to 90 ppm at 480 min. Only the traces of 4-MDBT and 3,6-DMDBT (less than 0.5 ppm) can be detected by GC-PFPD. 4-MDBT soared up to its maximum value after 60 min and gradually declined to zero after 420 min. On the other hand, the formation of 3,6-DMDBT was identified after 90 min and then increased linearly with time on stream. 4-MDBT may come from the trans-alkylation of the 4,6-DMDBT, while 3,6-DMDBT may come from the isomerization of the 4,6-DMDBT. Both reactions took place on acid sites of the zeolite, while HDS reaction occurred on the sulfided active metal sites. It has been reported that when the zeolite is introduced into the catalyst, the isomerization of the refractory S compounds reduces their steric hindrance and accelerates the HDS process [26]. Therefore, some HDS process may occur via a combination of isomerization and HDS reactions. That is, the most refractory S compounds first react with the acid sites to form isomers, and then, the intermediates further react on the active metal compounds.

In general, HDS is carried out through two parallel reactions [27]: DDS and HYD. For the DDS pathway, one of the double bonds in the vicinity of the sulfur atom undergoes partial hydrogenation to form a dihydro-intermediate. Then, a C–S bond is cleaved by an elimination process to form an SH group. The second C–S bond is broken to produce the final biphenyl-type compounds. For the HYD pathway, one aromatic ring is hydrogenated to create a tetrahydro methyl-substituted dibenzothiophene. The later one eliminates the C—S bond to form cyclohexylbenzene compounds. Normally, under HDS conditions, biphenyl type compounds are difficult to hydrogenate into cyclohexylbenzene [27]. When acid compounds, such as zeolite and silica-alumina were co-added into the support of CoMo or NiMo catalyst, addi-

tional reactions were observed, including (1) methylation of 4,6-DMDBT to form tri-, tetra-, penta-, and hexa-methyldibenzothiophenes; (2) isomerization of 4,6-DMDBT to 3,6-DMDBT or other methyl- position DMDBTs; (3) trans-alkylation of 4,6-DMDBT to methyldibenzothiophene and trimethyl dibenzothiophene, and (4) cracking of the desulfurized compounds to single-ring hydrocarbons. The isomerization reaction can profoundly affect the HDS, and it can shift the methyl groups from 4,6-position to the 3, 6 or other positions, which can reduce the steric hindrance between the molecule and catalyst active sites, therefore increasing the HDS reactivity [26].

Figure 8 shows the variation of the amounts of the toluene, benzene, methyl cyclohexane, and cyclohexane along with the reaction time over the CoMo/AZ catalyst.

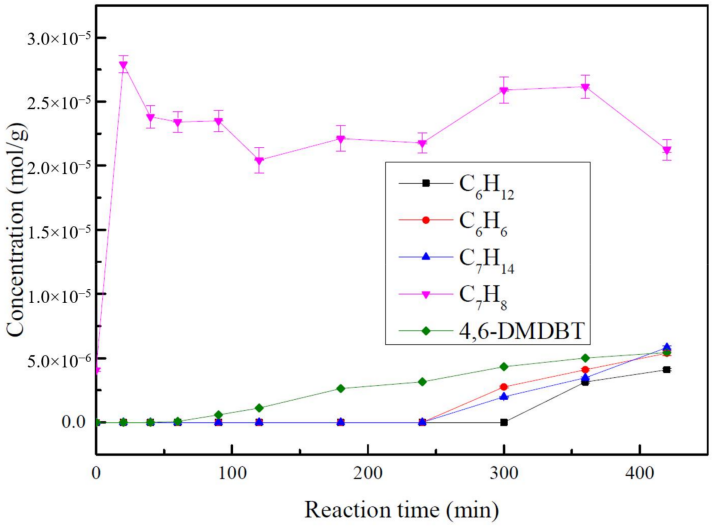

Figure 8. Concentrations of the products with time on stream over CoMo/AZ (reaction conditions: the same as the conditions in Figure 6).

According to the references, the HDS products from 4,6-DMDBT mainly includes: (1) 4,6-dimethyltetrahydrodibenzothiophere (4, 6-DMTHDBT) or 4,6-dimethyl hexahydrodibenzothiophere (4,6-DMHHDBT); (2) 3,3-dimethylbiphenyl (3,3′-DMBiP); (3) 3,6-dimethyldibenzothiophere (3,6-DMDBT); (4) 3,4′-dimethylbiphenyl (3,4′-DMBiP); (5) 3,3′-methylcyclohexy toluene (3,3′-MCHT); (6) 3,3′-dimethyl dicyclohexane; and (7) toluene and methylcyclohexane [28]. However, in our HDS studies, no double-cycle compounds, such as DMBP, MCHT, and DMDCH, were found in the final products, instead only toluene, benzene, cyclohexane, methyl cyclohexane, and trace 4-MDBT, 3,6-DMDBT, poly DMDBT were found by the GC-FID and GC-PFPD. The formation rate of toluene is significantly higher than that of the conversion of 4,6-DMDBT, indicating that most of the toluene is from the hydrocracking of 1-MN instead of the HDS process. Toluene can be formed either from the cracking of double-ring intermediate products in the 4,6-DMDBT HDS, such as 3,3′-DMBiP, 3,4′-DMBiP, as well as 3,3′-methylcyclohexy toluene, or from the hydrocracking of 1-MN [19,28]. Bataillie et al. did not find 3,3′-methylcyclohexy toluene in their final products and assumed that this compound may have been rapidly cracked into toluene and methylcyclohexane [26]. Furthermore, concentrations of benzene, methyl cyclohexane, and cyclohexane gradually increased with the reaction time, which might be caused by the hydrocracking of hydrogenated or partial hydrogenated double-ring intermediate products. On one hand, zeolite in the catalyst promotes the isomerization of 4,6-DMDBT to 3,6-DMDBT, improving both DDS and HYD reactivities [26]. On the other hand, a high zeolite content (30 wt%) will crack these double-ring products into the monocyclic products. In this study, it is difficult to differentiate between the DDS and HYD pathways in the HDS process because of the lack of intermediate reactants observed in the HDS products.

Effects of Nitrogen Introduction on HDS Performance

Figure 9 shows the variations of Ln(C_S) (the concentration of total sulfur) with the reaction time over the NiMo/AZ, CoMo/AZ, and NiW/AZ catalysts.

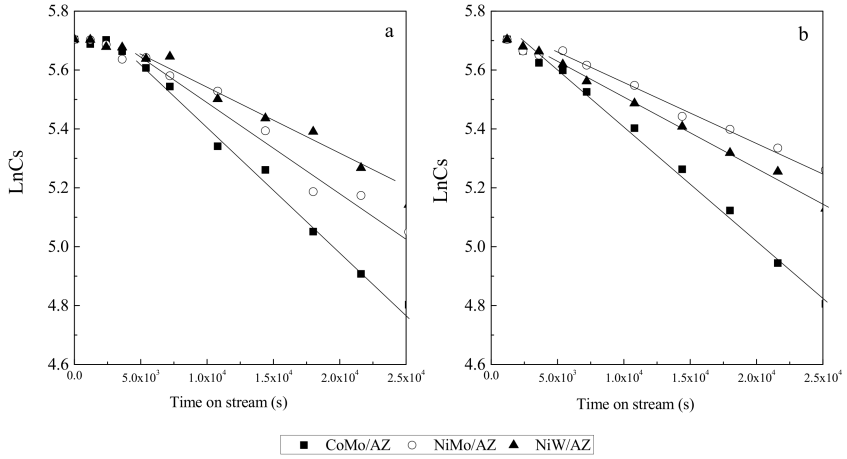

Figure 9. The effects of nitrogen introduction on Ln(C_s) with time on stream (Reaction conditions: 648 K, 8.96 MPa, 1000 rpm, 20 g catalyst, 200 g feed (4,6-DMDBT with 300 ppm sulfur, carbazole with 300 ppm nitrogen, 20 w% 1-MN in Hexadecane). (**a**) before the Nitrogen introduction; (**b**) after the Nitrogen introduction.

After the initial induced period to form active NiMoS, CoMoS, and NiWS phase, the concentration of 4,6-DMDBT decreased linearly. The HDS reaction of 4,6-DMDBT followed pseudo-first order kinetics and the plots of ln(Cs) versus time were always linear during the reaction time (when the catalyst activity is low).

Figure 9b shows the curves of Ln(C_S) versus the reaction time over the NiMo/AZ, CoMo/AZ, NiW/AZ catalysts after N (carbazole) was introduced. The kinetics rate constants of HDS reaction are listed in Table 3.

Table 3. The effects of Nitrogen introduction on the HDS kinetic rate constants.

$k_1 \times 10^{-5}$, s^{-1}·$gcat^{-1}$	CoMo/AZ	NiMo/AZ	NiW/AZ
Model 1 without N	4.37	3.07	2.48
Model 2 with N	3.87	2.09	2.25

CoMo/AZ showed the highest HDS kinetic rate constant, which decreased in the following order: CoMo/AZ > NiMo/AZ > NiWAZ. Due to the same support, the HDS reactivity of CoMo/AZ, NiMo/AZ, and NiW/AZ was determined by their hydrogenation ability and DDS ability. Under the low H_2 pressure at 550 psi, the preferred reaction route is the DDS pathway rather than HYD, therefore, CoMo/AZ has the highest DDS performance among the three catalysts. This is probably related to surface area, pore volume, micropore volume, the number of crystal slab layers, and the B acids on catalysts. These results are in good accordance with the DFT calculation results [18].

Even after being added the N compounds, CoMo/AZ still gave a higher kinetic rate constant value than NiMo/AZ and NiW/AZ, even those without N addition.

Although zeolite can isomerize most of the refractory S compounds and reduce the steric hindrance of the reactants, most of the S compounds were still converted via the DDS or HYD route. Therefore, N compounds might reduce the HDS activity by competing for the acidic sites on the zeolite, and reducing the activity of the isomerization reaction. However, N does not alter the reactive NiMoS, CoMoS, and NiWS phase, nor participate in the reaction, or change the reaction mechanism. Furthermore, after 300 ppm N (carbazole) was introduced, the kinetic constant rate of three catalysts decreased to 0.50 s^{-1}, 0.98 s^{-1}, and 0.23 s^{-1}, respectively. The results disclose that the poisoning of the N compounds on

the CoMo/AZ, NiMo/AZ, and NiW/AZ is different, which may be relative to the weak B acids on each catalyst.

HDA of 1-MN

Figure 10 shows that the selectivity of the products varied with the reaction time over the CoMo/AZ catalyst.

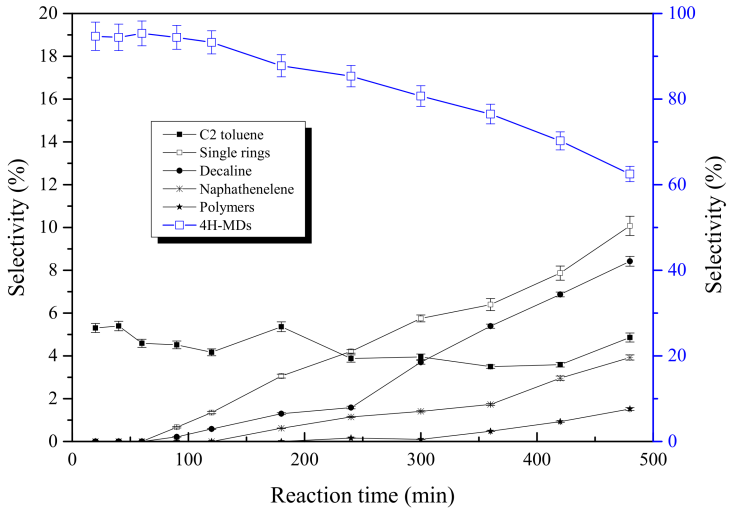

Figure 10. Distribution of 1-MN hydrogenated products with time on stream over CoMo/AZ (reaction conditions: the same as the conditions in Figure 8).

The major products include: (1) partially hydrogenated products, 1-, 2-, 5-, 6- methyltetralins (MT), (4H-MTs); (2) further hydrogenated products, decalins; (3) ring-opening products, single-rings; (4) cracked products, C2 toluene; and (5) condensation products, polymers. The selectivity of methyltetralins decreased while the other products increased with the reaction time, indicating that partially hydrogenated compounds are gradually transferred into the fully hydrogenated compounds. The results are also in accordance with the reports, where 1-MN was partially hydrogenated to methyldecalins at first and then further converted through hydrogenation, cracking, and isomerization reactions.

During the hydrogenation reactions, 1-MN was firstly partially hydrogenated to 1-, 2-, 5-, 6-MT. 1- and 5- are the direct hydrogenated products, and 2-, 6-MT are their isomerization products. After that, those were further hydrogenated, reconstructed, or cracked into different products [19].

The selectivity of 1-, 2-, 5-, and 6-MT in the 4H-MT products along with the reaction time is shown in Figure 11.

The selectivity of these 4H-MT products decreased in the following order: 5-MT > 1-MT >> 6-MT > 2-MT. The results suggest that direct hydrogenation is still the dominant process in the hydrogenation of 1-MN. With the reaction time increasing, more 2-MT and 6-MT increased, while the selectivity of 1-MT and 5-MT decreased, indicating that isomerization reaction is a secondary reaction following the hydrogenation reaction. Furthermore, the selectivity of 5-MT is higher than that of the 1-MT, suggesting that the hydrogenation reaction favors the aromatics rings without methyl group, which is consistent with the previously reports [19,29].

Hydrogenation of 1-MN

Figure 12 shows the hydrogenation of 1-MN over the CoMo/AZ, NiMo/AZ, and NiW/AZ catalysts.

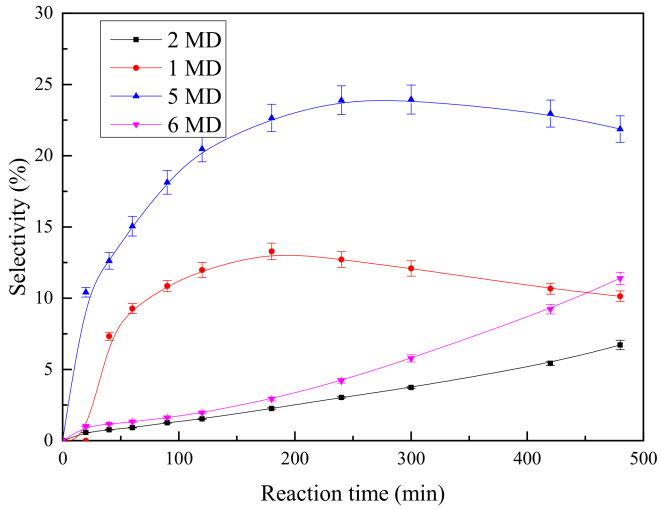

Figure 11. Selectivity of MTs with time on stream over CoMo/AZ (reaction conditions: the same as the conditions in Figure 8).

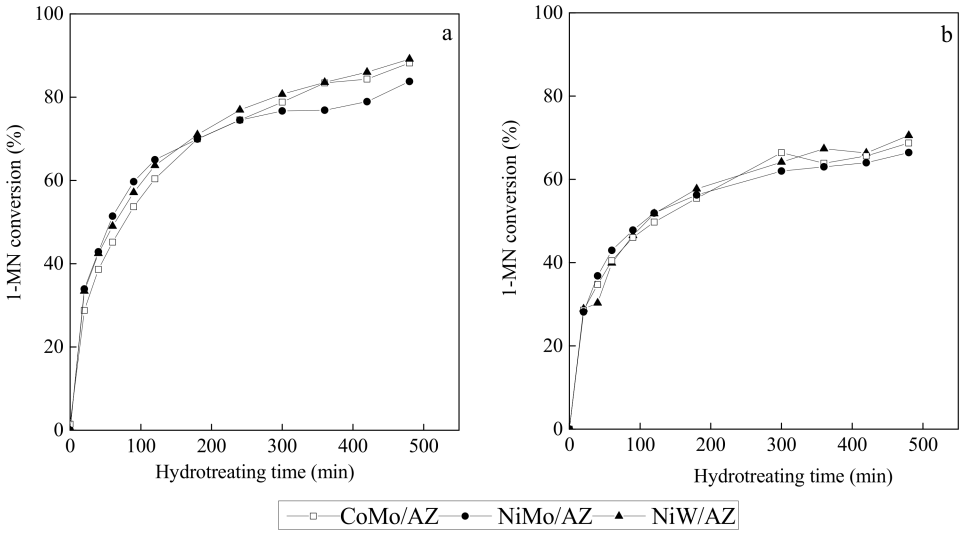

Figure 12. Hydrogenation of 1-MN with time on stream (reaction conditions: the same as the conditions in Figure 8). (**a**) without N compounds; (**b**) with 300 ppmN carbazole.

A similar trend in the conversion of 1-MN was established for all three catalysts. NiMo/AZ and NiW/AZ catalysts were supposed to have higher hydrogenation performances than CoMo/AZ; however, under low H_2 pressure at 550 psi, the catalysts may lose their superior hydrogenation ability. When the nitrogen was added into the feed, the conversion of 1-MN decreased significantly. As reported, nitrogen species affected both the acidic sites and hydrogenation sites, which reduced the hydrogenation activity of the catalysts [27].

Table 4 shows the yield of hydrogenation products from 1-MN at 480 min.

The NiMo/AZ catalyst had the highest yields of 1-MT and 5-MT and relatively lower yields of 2-MT and 6-MT, suggesting that the NiMo/AZ catalyst has higher hydrogenation ability. This may be related to the abundant acidic sites distributed on NiMo/AZ. When N was introduced into the feed, the yield of 1-MT and 5-MT increased, and the yield of 2-MT and 6-MT decreased. N might poison the zeolite active sites and reduce the isomerization of 1-MT and 5-MT, which in turn increases the direct hydrogenation of 1-MN. For all these three catalysts, the yield of 5-MT is higher than 1-MT, further suggesting that methyl groups reduce the hydrogenation of the aromatic groups. The yields of 2-MT and 6-MT are relatively lower over NiMo/AZ, suggesting a higher isomerization over CoMo/AZ

and NiW/AZ. Furthermore, the yields of single-ring products from the CoMo/AZ and NiW/AZ catalytic reaction are higher than that from the NiMo/AZ, due to the higher cracking ability of the former two catalysts.

Table 4. Chemical compositions of 1-MN hydrogenated products at 480 min.

Compositions, %	Model 1 without Nitrogen			Model 2 with Nitrogen		
	CoMo/AZ	NiMo/AZ	NiW/AZ	CoMo/AZ	NiMo/AZ	NiW/AZ
1-MT	10.1	14.1	9.7	16.3	17.9	15.5
2-MT	6.7	4.4	7.6	3.3	1.7	3.9
5-MT	21.9	27.4	22.1	30.3	33.9	29.4
6-MT	11.4	6.3	12.6	2.4	4.2	4.9
4H-HC	-	-	-	-	-	-
decalin	8.4	7.1	8.1	5.6	4.2	6.1
single ring	10.1	7.3	8.2	5.1	4.3	6.0
C2 toluene	4.9	5.6	5.2	5.1	4.6	5.0
naphathalene	3.9	3.1	4.0	2.7	2.5	2.9
polymer	1.5	0.6	1.4	1.1	0.9	1.2

2.2.2. Real LCO as Feed

The hydrotreating performances of NiMo/AZ, CoMo/AZ, and NiW/AZ with different LCO feeds are summarized in Tables 5 and 6.

Table 5. Sulfur content (ppm)in the final products with different LCO feed.

Feed	Catalyst	375 °C 1100 psig	375 °C, 550 psig	300 °C, 1100 psig
LCO1	CoMo/AZ	877	1016	2845
	NiMo/AZ	722	909	3198
	NiW/AZ	1121	1099	3538
LCO2	CoMo/AZ	586	1096	2334
	NiMo/AZ	512	612	2430
	NiW/AZ	567	958	3022

LCO1: sulfur 1.3% S; LCO2: sulfur 1.5% S.

Table 6. Nitrogen (ppm) content in the final products with different LCO feed.

Feed	Catalyst	375 °C, 1100 psig	375 °C, 550 psig	300 °C, 1100 psig
LCO1	CoMo/AZ	104.6	265.2	415.2
	NiMo/AZ	55.0	192.4	327.4
	NiW/AZ	83.8	208.7	378.4
LCO2	CoMo/AZ	14.5	49.7	93.1
	NiMo/AZ	5.4	17.6	57.3
	NiW/AZ	4.0	22.4	69.7

LCO1: 500 ppm N; LCO2: 140 ppm N.

As shown in Table 5, NiMo/AZ and CoMo/AZ showed different HDS performances when the reaction temperature was changed. At lower temperature (300 °C, 1100 psi), the residue S in the products with CoMo/AZ catalyst is 2334 ppm, which is slightly lower than that of the NiMo/AZ catalyst (2430 ppm S). However, at higher temperature (375 °C, 1100 psi), the residue sulfur in the products with CoMo/AZ (586 ppm) is higher than that with NiMo/AZ (512 ppm). Under lower reaction temperature, compared to NiMo/AZ, the HDS activity of CoMo/AZ is higher [5]. CoMo/AZ primarily catalyzes the DDS route. NiMo/AZ, on the other hand, primarily catalyzes the HYD route and shows a better hydrogenation performance. Even at 375 °C, 550 psi, the HDS activity of the NiMo/AZ was still close to that at 375 °C, 1100 psi, indicating that NiMo/AZ has a such high hydrogenation activity that it did not need high hydrogen pressure to achieve a higher total HDS activity.

Comparing the results of the NiMo/AZ and NiW/AZ catalysts, the HDS performances of NiMo/AZ is always higher than that of the NiW/AZ catalyst, which may be due to their different acid properties.

Combined Tables 1 and 5, the HDS activity is probably relevant to the length of slabs: the shorter of the crystal slab length is, the higher HDS activity of the catalyst has. The HDS activity under low reaction temperature is in accordance with the pore type: the more intra-aggregated pores on the catalyst, the higher HDS activity performance of the catalyst.

During the HDS reaction, the refractory S compounds are normally converted via the DDS and HYD pathways [27]. NiMo/AZ isomerizes more 4,6-DMDBT into 3,6-DMDBT, and increases the HDS activity of the catalyst more than the NiW/AZ does. Furthermore, from the TEM of sulfurized NiMo/AZ and NiW/AZ catalyst, it was found that NiMo/AZ had more 2–3-layer slabs than the NiW/AZ catalyst. It is believed that the multi-layered MoS_2 clusters have more multi-vacancies than single-layered clusters, thereby facilitating better adsorption of the aromatic ring [19]. Compared to NiW/AZ, the larger layer number of MoS_2 clusters on NiMo/AZ provides better isomerization, hydrogenation, and HDS performances. In addition, the shorter length of the slabs, the more brim sites on the surface of the catalyst, and the higher hydrogenation activity the catalyst.

As shown in Table 6, the HDN performances of the investigated catalysts was NiMo/AZ > NiW/AZ > CoMo/AZ under all three reaction conditions. The HDN reactions were carried out in a concessive process. The N aromatics are hydrogenated; then the C-N bonds are eliminated [30]. Therefore, the catalyst with high hydrogenation ability and suitable acid sites has a higher HDN performance. As discussed above, the NiMo/AZ catalyst presents higher hydrogenation ability than the NiW/AZ. Furthermore, it is known that Co-promoted catalysts have less hydrogenation ability than Ni-promoted catalysts; therefore CoMo/AZ has the lowest HDN activity among the three catalysts.

For higher N content in LCO1 feed, both HDS and HDN showed a similar trend that NiMo/AZ had a better HDS performance at high temperature and CoMo/AZ a better HDS performance at low temperature. Furthermore, at all reaction conditions, the HDN performances decrease in the following order: NiMo/AZ > NiW/AZ > CoMo/AZ, which is the same as the results from LCO2 tests.

Figures 13 and 14 present the hydrocarbon distributions in hydro-upgrading products.

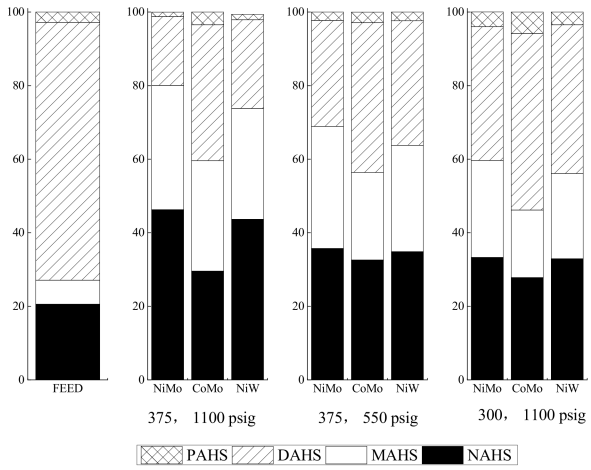

NiMo/AZ: NiMo; CoMo/AZ: CoMo; NiW/AZ: NiW
Poly-cyclic aromatics: PAHS; Di-ring aromatics: DAHS; Mono-ring aromatics: MAHS; Non-aromatics: NAHS

Figure 13. Hydrocarbon distributions in the final product with LCO1 feed.

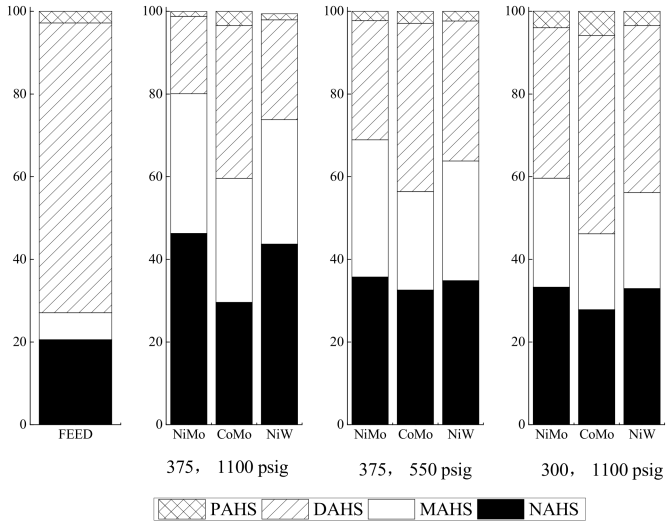

NiMo/AZ: NiMo; CoMo/AZ: CoMo; NiW/AZ: NiW.
Poly-cyclic aromatics: PAHS; Di-ring aromatics: DAHS; Mono-ring aromatics: MAHS; Non-aromatics: NAHS

Figure 14. Hydrocarbon distributions in the final product with LCO2 feed.

About 70% of LCO1 consisted of di-ring aromatics (DAHS). After the reaction, most of the DAHS were converted into mono-aromatics (MAHS) or non-aromatics. The CoMo/AZ had the lowest HDA activity. Non-aromatics (NAHS) were only produced in a concentration of 7–11%, and the rest of the non-aromatics are from the feed. When the pressure was low (550 psi), NiMo/AZ and NiW/AZ only showed slightly higher hydrogenation activities than the CoMo/AZ. However, when the reaction temperature and pressure were increased high enough, the NiMo/AZ and NiW/AZ catalyst showed significantly better hydrogenation performances than the CoMo/AZ, confirming that Ni-promoted catalysts have a greater hydrogenation performance than CoMo/AZ. Figure 14 shows that for the LCO1 feed with a higher N content, the HDA behaved the same to the previous report that at high temperature and high pressure, NiMo/AZ and NiW/AZ catalysts show significantly better hydrogenation performances than the CoMo/AZ. While at low pressure, NiMo/AZ and NiW/AZ show similar HDA performance to that of CoMo/AZ.

It was reported that the Bronsted acids were related to isomerization and ring opening reactions when aromatics were hydro-upgraded over bifunctional catalysts [31]. As can be seen in Figure 6 and Table 2, the sulfided NiMo/AZ and NiW/AZ catalysts have a similar total amount of Bronsted acid sites. This is in accordance with the results shown in Figures 13 and 14, where NiMo/AZ and NiW/AZ catalysts have similar HDA performances.

3. Experimental

3.1. Catalyst Preparation

The procedures of catalyst preparation are the same to our previous publications [15–17]. Zeolite HY, NH_4NaY (Zeolyst CBV-300) firstly underwent ammonia exchanging with NH_4Cl aqueous solution at 363–368 K for 1 h, and then dried at 383 K overnight. Zeolite-beta (Zeolyst CP814E) was calcined at 813 K for 10 h, and then hydrothermally treated in an autoclave at 823 K and 0.2 MPa for 2 h. The catalysts were prepared by mixing zeolite HY, zeolite beta, alumina, $Ni(NO_3)_2{\cdot}6H_2O$ or $Co(NO_3)_2{\cdot}6H_2O$, MoO_3 or $(NH_4)_6H_2W_{12}O_{40}$ with binder (SASOL, CAPAPAL B) in a HCl solution until distributed evenly. The mixture is then extruded to form a cylindrical shape, dried at 393 K for 2 h, and calcined in the air at 773 K for 4 h. The components of the above catalysts contain 5 wt% of NiO or CoO, 15 wt% of MoO_3 or

24 wt% of WO_3, 15 wt% of zeolite HY, 5 wt% of zeolite-beta, 20 wt% of binder (Al_2O_3), and 31–40 wt% Al_2O_3. The molar ratio of Ni (or Co)/Mo (or W) was 0.64.

Before each run, the catalysts were pre-sulfided in-situ with dimethyl disulfide (DMDS) at 593 K for 2 h, and then the temperature was increased up to 633 K and maintained for another 2 h.

3.2. Catalyst Characterization

The procedures of catalyst characterization are the same to our previous publications [15–17]. Nitrogen adsorption measurements were performed on a Quantachrome Autosorb-1 (Quantachrome Instrument, Boynton Beach, FL, USA). Before adsorption, the samples were calcined at 823 K for 16 h, and 20 to 40 mesh samples were degassed at 473 K and 1.33×10^{-3} Pa for 2 h, then adsorbed and desorbed at a temperature of 77 K. Surface area was calculated with the multipoint BET equation with linear region in the P/P_0 range of 0.05 to 0.35. Pore volume was calculated from the maximum adsorption amount of nitrogen at $P/P_0 = 0.99$. The pore size distribution was determined based on the BJH method and the desorption branch of the isotherm, and t-method was adopted for the micropore analysis.

X-ray powder patterns of the three sulfided catalysts were measured using a Bruker D8 Advance spectrometer (Bruker Corp., Billerica, MA, USA). The X-ray source was a 2.2 kW Cu X-ray tube, which is sealed and maintained at an operating current of 40 kV and 30 mA. Samples were scanned in the range of 5–80 (2θ) at a step size of 0.02.

Adsorbed pyridine infrared spectra (Pyridine-IR) were recorded on a NICOLET 6700 Spectrometer (Thermo Fisher Scientific, Waltham, MA, USA). Fifteen milligrams of grounded samples were pressed to form 1 cm wafers and then preheated to 723 K under vacuum (2–3 Torr) for 2 h. Pyridine was introduced and evacuated under vacuum at 423 K. Infrared spectra were recorded at desorption of 423 K, 523 K, 623 K, and 723 K, respectively.

TEM was performed on a JEOL 2010 STEM (JEOL Ltd., Mitsuko, Tokyo, Japan), operating at 200 keV. The spectra were collected using an EDAX Genesis 4000 system. A small amount of sulfided catalyst powder was sonicated in 100% ethanol, and then one drop of it was taken with a micropipette and dropped onto a copper (or nickel) support grid. The average slab length was measured using image analysis software, and the average sizes were calculated based on 100+ slabs of various particles.

The types and strengths of acids on the surfaces of catalysts were tested by Pyridine FTIR. Infrared spectra were recorded on a Nicolet FTIR-6700 (Thermo Fisher Scientific, Waltham, MA, USA) at temperatures of 150, 250, and 350 °C. The characteristic bands at 1450 cm^{-1} and 1550 cm^{-1} were respectively assigned to Lewis(L) and Bronsted (B) acid sites [32]. The ratio of L acids to B acids was calculated by the method used in the literature [33].

The XPS measurements were carried out on an ESCALAB 250Xi spectrometer (Thermo Fisher Scientific, Waltham, MA, USA) equipped with a pass energy of 30 eV with a power of 100 W (10 kV and 10 mA) and a monochromatized AlKα X-ray (hν = 1486.65 eV) source.

3.3. Catalyst Evaluation

The catalyst reaction performances were evaluated with the same procedures to our previous publications [15–17]. The model compounds, 4,6-DMDBT and 1-methylnaphthlene (1-MN) were tested using hexadecane as the solvent (named as Model 1). Then carbazole (named as Model 2) was introduced to investigate the effects of nitrogen on HDS and HDA. The concentration of total sulfur and nitrogen were 300 ppmw, and 1-MN was 20 wt%. The catalyst activity was evaluated in a 1 L of stirred autoclave (Autoclave Engineers). Twenty grams of catalyst was loaded in the catalyst basket of the reactor and filled with H_2. The catalyst was sulfided with DMDS at 593 K for 2 h and 633 K for another 2 h, and then 200 g of LCO was charged into the autoclave, which was stabilized at 8.96 MPa and 648 K with a stirring rate of 1000 rpm.

The catalyst reaction performances were then evaluated with a 20 mL fixed-bed microreactor. Two kinds of LCO feed (named as LCO1 and LCO2, respectively) were used in this study. The catalyst sulfidation procedures were the same to the above-mentioned conditions. The hydrogen flow rate was 30 standard-state cubic centimeter per minute (SCCM) and the liquid hourly space velocity (LHSV) is 0.6 h^{-1} (these conditions were held constant). The reaction conditions were 648 K with 1100 psig, 648 K with 550 psig, and 573 K with 1100 psig, respectively.

The hydro-upgrading liquids were analyzed by GC/MS and GC/PFPD. The total nitrogen and sulfur contents as well as the aromatic contents were respectively tested by ASTM D 4629 and ASTM D 4294, and ASTM D 6591 standards.

As the cracking degree of hexadecane was lower than 5 wt% under the investigated conditions, the effects of hexadecane cracking reactions were neglected.

4. Conclusions

The hydrotreating performances of NiMo/AZ, CoMo/AZ, and NiW/AZ were investigated on both model compounds and real LCO.

At 375 °C and 550 psi, the HDS activity of these catalysts decreased in the order: CoMo/AZ > NiMo/AZ > NiW/AZ. When the H_2 pressure is low, the HYD pathways were limited and CoMo catalysts showed a higher HDS performance. The addition of nitrogen compounds in the feed introduces a competitive adsorption mechanism and leads to reduction of the amount of acid sites used for isomerization. CoMo/AZ still shows the highest HDS performances among the three catalysts after carbazole was introduced into the feed. Direct hydrogenation is still the dominant process in the partial hydrogenation of 1-MN into the 1MTs. Isomerization and cracking reactions were reported as the secondary reactions. The different active metal compounds change the ratio between the hydrogenation, cracking, and isomerization. Hydrogenation reactions occur more frequently on the benzene-ring without methyl group sides.

The HDS performances of the catalyst were influenced by hydrogenation ability and acid properties of the catalyst. When LCO was used as the feed, CoMo/AZ showed better HDS performance at low temperature and NiMo/AZ showed higher HDS activity at high temperature. Between NiMo/AZ and NiW/AZ, the sulfurized NiMo/AZ has more acid sites than the sulfurized NiW/AZ. Thus NiMo/AZ isomerized more 4, 6 DMDBT into 3,6 DMDBT, and then increased the activity of the catalyst. HDN performances decreased in the order NiMo/AZ > NiW/AZ > CoMo/AZ. Under low temperature and low pressure, the HDA performances of NiMo/AZ and NiW/AZ are slightly higher than that of the CoMo/AZ. Under higher H_2 pressure, the HDA of NiMo/AZ and NiW/AZ was significantly improved, greatly higher than that of the CoMo/AZ.

Author Contributions: Conceptualization, H.W. (Hui Wang), H.Z. and S.N.; data curation, H.W. (Hui Wang), J.P. and M.W.; formal analysis, H.W. (Hui Wang), J.P. and M.W.; funding acquisition, H.W. (Hui Wang) and J.P.; investigation, H.W. (Hui Wang), J.P., M.W. and H.Z; methodology, H.W. (Hui Wang) and H.Z.; project administration, H.W. (Hui Wang) and H.Z.; resources, H.W. (Hui Wang) and H.Z.; software, H.W. (Hui Wang) and H.Z.; supervision, H.W. (Hui Wang) and H.Z.; validation, H.W. (Hui Wang), J.P., M.W. and H.Z.; visualization, H.W. (Hui Wang) and H.Z.; writing—original draft, H.W. (Hui Wang), K.R., P.S. and H.Z.; writing—review and editing, H.W. (Hui Wang), J.P., H.Z., K.R., S.N., H.W. (Hongmei Wang) and P.S. All authors have read and agreed to the published version of the manuscript.

Funding: This research was funded by the Natural Science Foundation of Zhejiang Province, China (Grant No. LQ20B060008); Jiaxing University, grant number #70518034/CD70518034.

Conflicts of Interest: The authors declare no conflict of interest.

Abbreviations

LCO	Light cycle oil
CN	Cetane number
AZ	Alumina-zeolite
DDS	Direct desulfurization
HYD	hydrogenation
HDS	Hydrodesulfurization
HDN	Hydrodenitrogenation
HDA	Hydrodearomatization
FCC	Fluid catalytic cracking
PAH	Polycyclic aromatic hydrocarbons
GC	Gas chromatography
FID	Flame Ionization Detector
PFPD	Pulsed flame photometric detector
GC/MS	Gas chromatography and mass spectrometry
HPLC	High performance liquid chromatography
XRD	X-ray diffraction
FTIR	Fourier transform infrared spectroscopy
XPS	X-Ray Photoelectron Spectroscopy
TEM	Transmission electron microscopy
DMDBT	Dimethyl dibenzothiophene
LHSV	Liquid hourly space velocity
1-MN	1-methylnaphthlene
S	Sulfur
N	Nitrogen
MDBT	Methyl dibenzothiophene
4,6-DMTHDBT	4,6-dimethyltetrahydrodibenzothiophere
4,6-DMHHDBT	4,6-dimethylhexahydrodibenzothiophere
3,3′-DMBiP	3,3-dimethylbiphenyl
3,6-DMDBT	3,6-dimethyldibenzothiophere
3,4′-DMBiP	3,4′-dimethylbiphenyl
3,3′-MCHT	3,3′-methylcyclohexy toluene
IS	Initial state
TS	Transition state
FS	final states
EB	Energy barrier
Cs	Concentration of sulfur
MT	Methyltetralins
PAHS	Poly cyclic aromatics
DAHS	Di-ring aromatics
MAHS	Mono-ring aromatics
NAHS	Non-aromatics

References

1. Shi, Q.; Zhao, S.; Zhou, Y.; Gao, J.; Xu, C. Development of heavy oil upgrading technologies in China. *Rev. Chem. Eng.* **2020**, *36*, 1–19. [CrossRef]
2. Peng, C.; Fang, X.C.; Zeng, R.H.; Guo, R.; Hao, W.Y. Commercial analysis of catalytic hydroprocessing technologies in producing diesel and gasoline by light cycle oil. *Catal. Today* **2016**, *276*, 11–18. [CrossRef]
3. Peng, C.; Yang, X.; Fang, X.; Huang, X.; Cheng, Z.; Zeng, R.; Guo, R. Development of Light Cycle Oil (LCO) Hydrocracking Technology over a Commercial W-Ni Based Catalyst. *China Pet. Process. Petrochem. Technol.* **2015**, *17*, 30–36.
4. Zhang, Z.; Zhang, W.; Zhang, Y.; Ji, D.; Jin, H.; Wang, G.; Zhang, Z. Technical review on flexible processing middle distillate for achieving maximum profit in China. *Appl. Petrochem. Res.* **2017**, *7*, 67–77. [CrossRef]
5. Knudsen, K.G.; Cooper, B.H.; Topsoe, H. Catalyst and process technologies for ultra low sulfur diesel. *Appl. Catal. A Gen.* **1999**, *189*, 205–215. [CrossRef]
6. Hu, W.; Zhang, H.; Wang, M.; Pu, J.; Rogers, K.; Wang, H.; Ng, S.; Xu, R. Hydro-upgrading of light cycle oil-synthesis of NiMo/SiO2-Al2O3-TiO2 porous catalyst. *J. Porous Mater.* **2021**, *28*, 867–874. [CrossRef]

7. Zhou, W.; Zhang, Q.; Zhou, Y.; Wei, Q.; Du, L.; Ding, S.; Jiang, S.; Zhang, Y. Effects of Ga- and P-modified USY-based NiMoS catalysts on ultra-deep hydrodesulfurization for FCC diesels. *Catal. Today* **2018**, *305*, 171–181. [CrossRef]
8. Naranov, E.R.; Sadovnikov, A.A.; Maximov, A.L.; Karakhanov, E.A. Development of micro-mesoporous materials with lamellar structure as the support of NiW catalysts. *Microporous Mesoporous Mater.* **2018**, *263*, 150–157. [CrossRef]
9. Ding, L.; Zheng, Y.; Zhang, Z.; Ring, Z.; Chen, J. Hydrotreating of light cycled oil using WNi/Al2O3 catalysts containing zeolite beta and/or chemically treated zeolite Y. *J. Catal.* **2006**, *241*, 435–445. [CrossRef]
10. Ding, L.; Zheng, Y.; Zhang, Z.; Ring, Z.; Chen, J. Hydrotreating of light cycle oil using WNi catalysts containing hydrothermally and chemically treated zeolite Y. *Catal. Today* **2007**, *125*, 229–238. [CrossRef]
11. Ding, L.; Zheng, Y.; Yang, H.; Parviz, R. LCO hydrotreating with Mo-Ni and W-Ni supported on nano- and micro-sized zeolite beta. *Appl. Catal. A Gen.* **2009**, *353*, 17–23. [CrossRef]
12. Ding, L.; Zheng, M.; Wang, A.; Zhang, T. A Novel Route to the Preparation of Carbon Supported Nickel Phosphide Catalysts by a Microwave Heating Process. *Catal. Lett.* **2010**, *135*, 305–311. [CrossRef]
13. Yao, S.; Zheng, Y.; Ding, L.; Ng, S.; Yang, H. Co-promotion of fluorine and boron on NiMo/Al2O3 for hydrotreating light cycle oil. *Catal. Sci. Technol.* **2012**, *2*, 1925–1932. [CrossRef]
14. Yao, S.; Zheng, Y.; Ng, S.; Ding, L.; Yang, H. The role of nanobeta zeolite in NiMo hydrotreating catalysts. *Appl. Catal. A Gen.* **2012**, *435*, 61–67. [CrossRef]
15. Ding, L. Hydrotreating Catalyst Supported on Modified Al_2O_3 and Zeolites for Hydroupgrading Light Cycle Oil. Ph.D. Thesis, University of New Brunswick, Fredericton, NB, Canada, 2006.
16. Zhang, H. Synthesis of Highly Active Unsupported Molybdenum Sulfide Catalysts for Hydrodesulfurization and Hydrodeoxygenation. Ph.D. Thesis, University of New Brunswick, Fredericton, NB, Canada, 2014.
17. Wang, H. Integration of Catalytic Cracking and Hydrotreating Technology for Triglyceride Deoxygenation. Ph.D. Thesis, University of New Brunswick, Fredericton, NB, Canada, 2016.
18. Zheng, P.; Li, T.; Chi, K.; Xiao, C.; Wang, X.; Fan, J.; Duan, A.; Xu, C. DFT insights into the direct desulfurization pathways of DBT and 4,6-DMDBT catalyzed by Co-promoted and Ni-promoted MoS2 corner sites. *Chem. Eng. Sci.* **2019**, *206*, 249–260. [CrossRef]
19. Wu, T.; Chen, S.-L.; Yuan, G.-M.; Pan, X.; Du, J.; Zhang, Y.; Zhang, N. High Metal-Acid Balance and Selective Hydrogenation Activity Catalysts for Hydrocracking of 1-Methylnaphthalene to Benzene, Toluene, and Xylene. *Ind. Eng. Chem. Res.* **2020**, *59*, 5546–5556. [CrossRef]
20. Wang, H.; Li, G.; Rogers, K.; Lin, H.; Zheng, Y.; Ng, S. Hydrotreating of waste cooking oil over supported CoMoS catalyst Catalyst-deactivation mechanism study. *Mol. Catal.* **2017**, *443*, 228–240. [CrossRef]
21. Cortes, J.C.; Rodriguez, C.; Molina, R.; Moreno, S. Hydrocracking of 1-methylnaphtalene (1MN) over modified clays-supported NiMoS and NiWS catalyst. *Fuel* **2021**, *295*, 120612. [CrossRef]
22. Dik, P.P.; Golubev, I.S.; Kazakov, M.O.; Pereyma, V.Y.; Smirnova, M.Y.; Prosvirin, I.P.; Gerasimov, E.Y.; Kondrashev, D.O.; Golovachev, V.A.; Kleimenov, A.V.; et al. Influence of zeolite content in NiW/Y-ASA-Al2O3 catalyst for second stage hydrocracking. *Catal. Today* **2021**, *377*, 50–58. [CrossRef]
23. Salam, M.A.; Cheah, Y.W.; Ho, P.H.; Olsson, L.; Creaser, D. Hydrotreatment of lignin dimers over NiMoS-USY: Effect of silica/alumina ratio. *Sustain. Energy Fuels* **2021**, *5*, 3445–3457. [CrossRef]
24. Santos, B.M.; Zhao, W.; Zotin, J.L.; da Silva, M.A.P.; Oliviero, L.; Mauge, F. Impact of proximity between NiMoS and zeolitic HY sites on cyclohexene hydroconversion: An infrared operando study of sulfide catalysts. *J. Catal.* **2021**, *396*, 92–103. [CrossRef]
25. Hu, E.; Yao, Z.; Zhao, L.; Wu, J.; Meng, H.; Huo, L.; Li, Y. Characteristics of zeolite-modified NiMo/Al2O3 catalysts and their hydrotreating performance for light cycled oil. *Can. J. Chem. Eng.* **2019**, *97*, 1107–1113. [CrossRef]
26. Laredo, G.C.; Merino, P.M.V.; Hernandez, P.S. Light Cycle Oil Upgrading to High Quality Fuels and Petrochemicals: A Review. *Ind. Eng. Chem. Res.* **2018**, *57*, 7315–7321. [CrossRef]
27. Chen, X.; Dong, Y.; Yu, X.; Wang, Z.; Liu, Y.; Liu, J.; Yao, S. Steric Hindrance of Methyl Group on the Reaction Pathway of Hydrodesulfurization in the Presence of Quinoline. *Catal. Lett.* **2021**, *151*, 194–211. [CrossRef]
28. Vega-Merino, P.M.; Quintana-Solorzano, R.; Laredo-Sanchez, G.C.; Arzate-Barbosa, E.; Olmos-Cerda, E.H. Impact of variables on the naphthalene hydrogenation for the tetralin formation towards BTX production. *Int. J. Oil Gas Coal Technol.* **2020**, *23*, 504–517. [CrossRef]
29. Cao, Z.; Zhang, X.; Xu, C.; Huang, X.; Wu, Z.; Peng, C.; Duan, A. Selective hydrocracking of light cycle oil into high-octane gasoline over bi-functional catalysts. *J. Energy Chem.* **2021**, *52*, 41–50. [CrossRef]
30. Tung, N.T.; Shnzaki, A.; Qian, E.W. Hydrodesulfurization, Hydrodenitrogenation and Hydrodearomatization over CoMo/SAPO-11-Al2O3 Catalysts. *J. Jpn. Pet. Inst.* **2017**, *60*, 301–310.
31. Peng, C.; Zhou, Z.; Cheng, Z.; Fang, X. Upgrading of Light Cycle Oil to High-Octane Gasoline through Selective Hydrocracking over Non-Noble Metal Bifunctional Catalysts. *Energy Fuels* **2019**, *33*, 1090–1097. [CrossRef]
32. Ward, J.W. Nature of active sites on zeolite. Rare earth Y zeolite. *J. Catal.* **1969**, *13*, 321–327.
33. Wu, X. *Acidity and Catalytic Activity of Zeolite Catalysts Bound with Silica and Alumina*; Texas A&M University: College Station, TX, USA, 2003.